ACS APPLIED MATERIALS & INTERFACES

www.acsami.org

Research Article

Exceptionally Fast Ion Diffusion in Block Copolymer-Based Porous Carbon Fibers

John P. Elliott, Naresh C. Osti,* Madhusudan Tyagi, Eugene Mamontov, Lifeng Liu, Joel M. Serrano, Ke Cao, and Guoliang Liu*

Cite This: *ACS Appl. Mater. Interfaces* 2022, 14, 36980−36986

Read Online

ACCESS | Metrics & More | Article Recommendations | Supporting Information

ABSTRACT: Confined ionic liquids in hydrophilic porous media have disrupted lattices and can be divided into two layers: An immobile ion layer adheres to the pore surfaces, and an inner layer exhibits faster mobility than the bulk. In this work, we report the first study of ionic liquids confined in block copolymer-based porous carbon fibers (PCFs) synthesized from polyacrylonitrile-*block*-polymethyl methacrylate (PAN-*b*-PMMA). The PCFs contain a network of unimodal mesopores of 13.6 nm in diameter and contain more hydrophilic surface functional groups than previously studied porous carbon. Elastic neutron scattering shows no freezing point for 1-butyl-3-methylimidazolium tetrafluoroborate ([BMIM]BF_4) confined in PCFs down to 20 K. Quasi-elastic neutron scattering (QENS) is used to measure the diffusion of [BMIM]BF_4 confined in PCFs, which, surprisingly, is 7-fold faster than in the bulk. The unprecedentedly high ion diffusion remarks that PCFs hold exceptional potential for use in electrochemical catalysis, energy conversion, and storage.

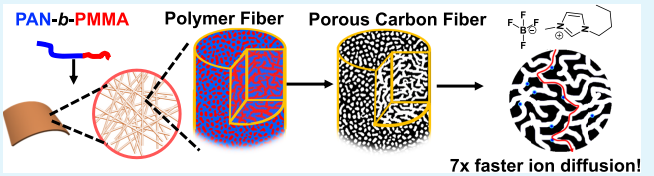

KEYWORDS: *block copolymer, porous carbon fiber, quasielastic neutron scattering, ion diffusion, room temperature ionic liquid*

1. INTRODUCTION

Fast diffusion is crucial for ions, molecules, and other chemical species to transport through materials such as polymers,[1,2] metal−organic frameworks, and covalent organic frameworks[3] and to participate in fast-kinetics electrochemical processes (*e.g.*, electrochemical reactions and diffusion-limited charging/discharging processes).[4,5] Room-temperature ionic liquids (RTIL) are attractive electrolytes because of their high stability.[6−8] Their strongly attractive intermolecular forces, however, reduce their diffusion and limit their use in diffusion-controlled processes.[9]

Frustrated by mismatched cation and anion sizes, RTIL form a weak lattice structure, allowing the ions to exist as liquids and diffuse at room temperature.[10] Nevertheless, compared with aqueous systems, the diffusion of RTIL is orders of magnitude slower. If the lattice structure is disrupted, the ion diffusion properties improve.[11] Therefore, nanopore-induced confinement is an effective method to increase ion mobility because it further weakens the lattice structure.[12] Toward confining ions, both pore size and interfacial interactions play a significant role. Too strong interactions between the ions and micropore surfaces lead to immobility of the former, forming a fixed surface ion layer that fills the whole pore. Given slightly larger pores, which accommodate more ion layers, the ions toward the center move independently of the fixed surface ion layer, decoupling them from the typical ionic liquid lattice. In general, pores of larger sizes can fit more ion layers in the centers, extending the effect of the disrupted ion lattice to improve the ion mobility. However, if the pore size is too large, the confinement effect diminishes, and the ion diffusion behavior approximates to that in the bulk. Therefore, the pore size must be small enough to disrupt the lattice structure but large enough to hold as many ions as possible to get the most benefit from confinement of the ions. Moreover, the pores should be as uniform and interconnected as possible to facilitate ion transport.

Block copolymer-based porous carbon fibers (PCFs) are emerging materials with unique hierarchical structures that allow easy accessibility to their large internal surface areas through their interconnected pores.[13−15] Similar to nonporous carbon fibers, the interwoven fibers form a mat with abundant interfiber spaces as macropores as well as micropores intrinsically defined by the interlayer distances of graphitic carbon. The effects of the confinement remain important for ionic liquid ordering.[16] Unique to PCFs, however, is a unimodal interconnected mesoporous network in each individual fiber, which acts as a network of channels to deliver ions to the internal micropores. Ion mobility in micropores is limited due to the lack of space for ion movement ($[BMIM]^+$ diameter, 3.8−5.8 Å),[17] but the mesopores provide significantly more space and allow for uninhibited ion diffusion.[18]

Received: July 17, 2022
Accepted: July 21, 2022
Published: August 2, 2022

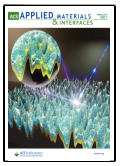

https://doi.org/10.1021/acsami.2c12755
ACS Appl. Mater. Interfaces 2022, 14, 36980−36986

The interconnected, hierarchical micro-, meso-, and macropores within PCFs facilitate ion diffusion and show distinct ion diffusion characteristics compared to other porous carbon materials.[19−21] The extra pore space is especially important for electrochemical applications, where ions in the fixed surface layer are mostly immobile, and the space away from the pore walls prevents clogging of the pores with the immobile ion layer.[22] Moreover, defined by the block copolymer molecular weight, the tunable mesopores offer sufficient space to hold non-surface layer ions, but are tight enough to disrupt the ionic lattice structure. Therefore, we hypothesize that the block copolymer-defined mesoporous structures will provide an exceptional porous network for enhanced ion diffusion.

To test this hypothesis, we synthesized block copolymer-based porous carbon fibers from polyacrylonitrile-*block*-polymethyl methacrylate (PAN-*b*-PMMA) and investigated the diffusion within. To quantify the ultimate capability of porous carbon fibers for ion diffusion, we chose a RTIL system of 1-butyl-3-methylimidazolium tetrafluoroborate ([BMIM]-BF_4). Self-diffusion of the [BMIM] cation both in the bulk and confined in porous carbon fibers was measured using quasi-elastic neutron scattering (QENS). Diffusion coefficients were compared to the literature for [BMIM] confined in porous media, and the block copolymer-based porous carbon fibers showed 7-fold faster ion diffusion than that in the bulk.

2. RESULTS AND DISCUSSION

Porous carbon fibers were synthesized according to an established method in our previous report (Figure 1a and Figure S1).[13] Briefly, PMMA was synthesized via reversible addition-fragmentation chain-transfer (RAFT) polymerization using cumyl dithiobenzoate (CDB) as the chain transfer agent. The purified PMMA (65.7 kDa, Đ = 1.08) was characterized by size exclusion chromatography (SEC) with both dynamic light scattering and refractive index detectors (Figure S2).

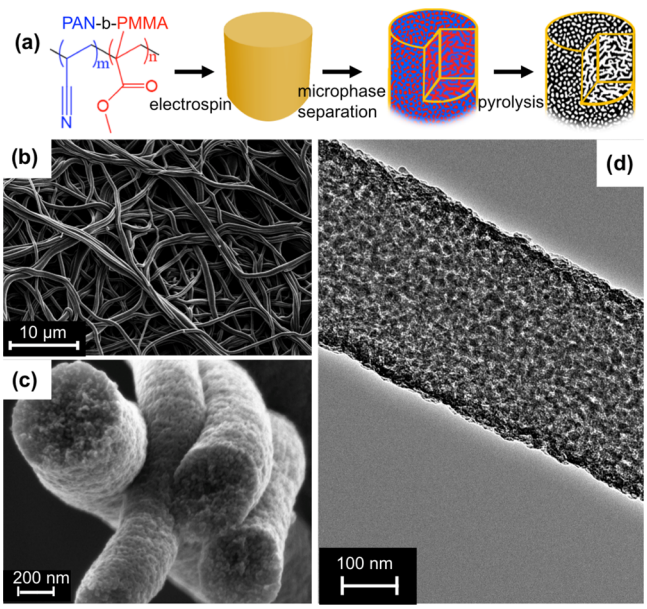

Figure 1. (a) Schematic illustration of the synthesis of PCFs from PAN-*b*-PMMA. (b) SEM image of a porous carbon fiber mat. (c) Cross-sectional SEM shows the uniform mesopores within each fiber. (d) TEM image illustrates internal porosity and interconnectivity of the porous network inside the fibers.

Then, the block copolymer was synthesized by chain extension of CDB-terminated PMMA using acrylonitrile. The resulting PAN-*b*-PMMA (136.7 kDa, Đ = 1.12) was purified and characterized by SEC (Figure S2) and ^{1}H NMR (Figure S3). Thermogravimetric analysis (TGA) in nitrogen showed a polymer char yield of 32% at 600 °C, and TGA simulating the fiber synthesis conditions produced a char yield of 31% (Figure S4). PAN-*b*-PMMA was electrospun into polymer fibers, which were oxidized at 280 °C for 8 h and then pyrolyzed at 800 °C for 1 h into porous carbon fibers. X-ray photoelectron spectroscopy (XPS) revealed the composition of the carbon fibers, which included 10.2% N and 4.1% O (Figure S5). Scanning electron micrography (SEM) showed the block copolymer-based porous carbon fiber mat possessed abundant macropores in between the fibers (Figure 1b). Within each fiber were interconnected mesopores, as evidenced by the cross-sectional SEM and TEM micrographs (Figure 1c,d). The porosity and general interconnectivity of the pores (Figure 1d) suggested a large easily accessible internal pore volume in PCFs.

It is well known that ionic liquids behave differently in confined environments, and QENS is incapable of differentiating between the confined and unconfined ion liquids. In other words, when a porous material is fully immersed in an ionic liquid, diffusion-controlled processes are measured as a combination of diffusion outside the material (non-confined) and inside the internal pores (confined). Therefore, a high volume of confined ionic liquid is required to maximize the signal of confined ion diffusion. Porous carbon fibers have high internal volumes within their mesoporous networks and thus are ideal for QENS measurement of ion diffusion under confinement. However, it is crucial to leave macropores void and fill only the mesopores and micropores with ions, properly confining the ionic liquid. Because macropores are generally too large to disrupt the lattice structure of an ionic liquid significantly, any ions in the macropores behave as if they are in bulk. To prepare for QENS measurement, we filled only the meso- and micropores with the ionic liquid using vacuum infiltration[23,24] by suspending PCFs in a solution of [BMIM]-BF_4 in acetonitrile (0.015 mg/mL). The suspension was stirred for 3 h at room temperature. Afterward, acetonitrile was removed by heating PCFs in an oven at 80 °C under a vacuum for 12 h.

Physisorption tests of both N_2 at 77.4 K and CO_2 at 273.2 K (Figure 2a,b) were performed before and after loading with [BMIM]BF_4 to confirm the occupation of the meso- and micropores. After loading [BMIM]BF_4, the N_2-sorbed surface area decreased from 404 ± 1 to 76 ± 1 m^2/g, as determined using the Brunauer−Emmett−Teller (BET) method. Based on non-local density functional theory (DFT), pore size distributions exhibited predominant micropore sizes of 0.55, 0.86, and 1.23 nm, as well as a mesopore peak at ∼13.6 nm (Figure 2c). Notably, all meso- and micropore sizes remained unchanged, but the total volumes decreased by ∼48.5%. The loading of the ionic liquid was not uniform throughout the pores because only about half of the pore volume was filled, but none of the neutron scattering data rely on uniformity of the ionic liquid. The neutron beam size is on the order of 10 cm^2 in area, and the neutron scattering data is only collected for neutrons that are scattered off of hydrogen atoms, negating any impact that may arise from non-uniformity. Physisorption relies on the accessibility of gas molecules to the pore surfaces. The reduced surface area and pore volume, in combination

https://doi.org/10.1021/acsami.2c12755
ACS Appl. Mater. Interfaces 2022, 14, 36980−36986

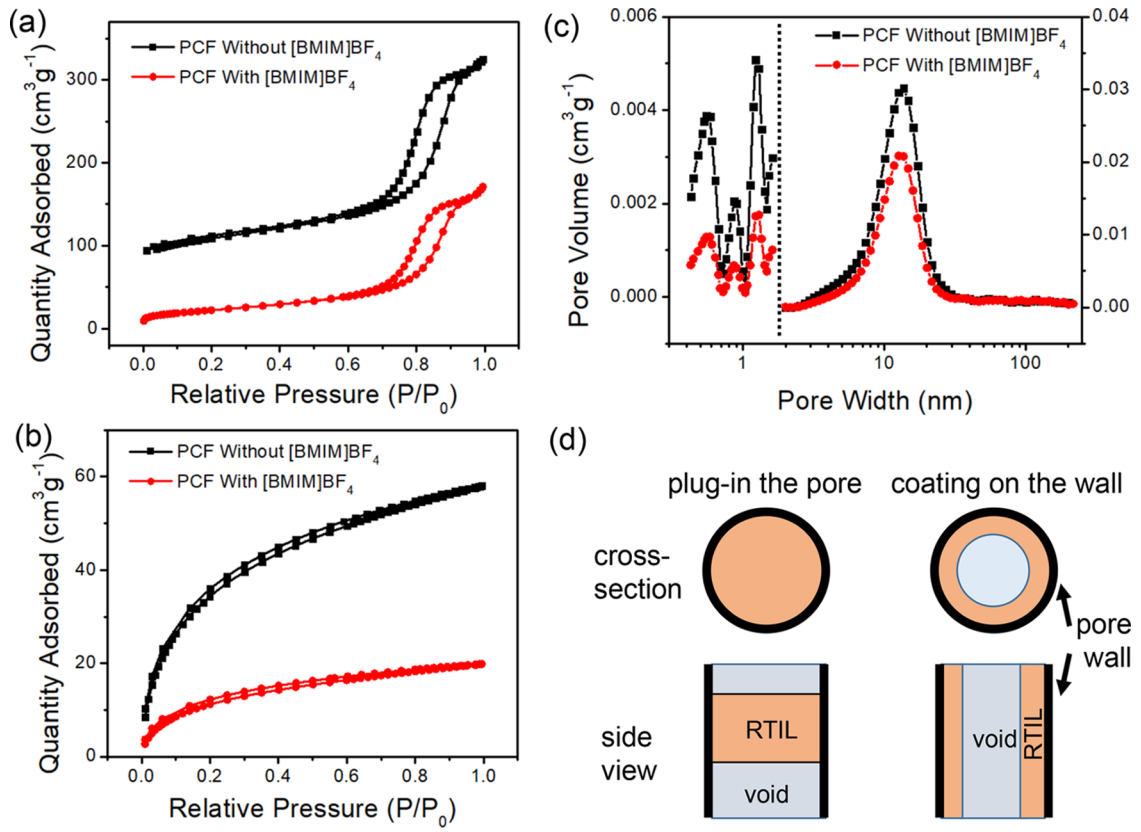

Figure 2. Representative (a) N_2 and (b) CO_2 physisorption isotherms (n = 1) before and after loading [BMIM]BF_4 into the porous carbon fibers. The reduced adsorbed quantities confirm the loading of the ionic liquid in the fibers. (c) Pore size distributions show that the ionic liquid occupied the pore volumes but did not change the pore sizes. (d) Physisorption suggests that [BMIM]BF_4 filled the pores as plugs (left) rather than coatings on the walls (right).

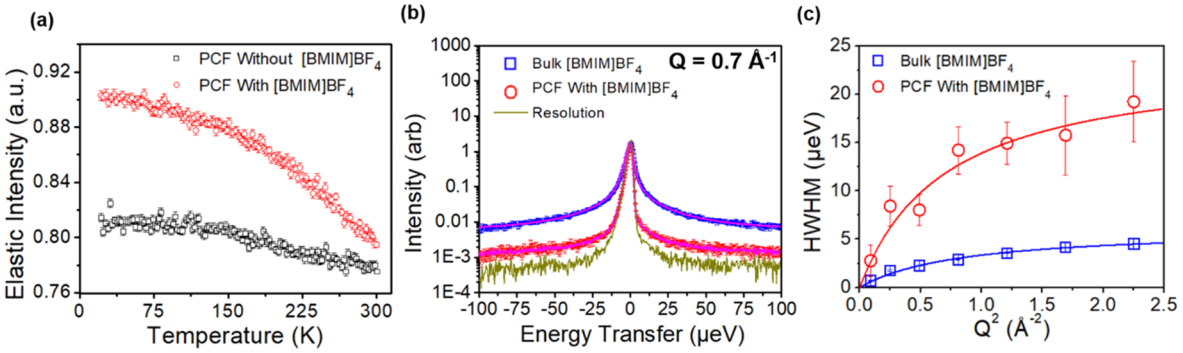

Figure 3. (a) Elastic scattering spectra of porous carbon fibers (n = 1) with and without [BMIM]BF_4. The enhanced elastic scattering intensity confirms that [BMIM]BF_4 was loaded into the pores. The lack of a thermal transition corresponding to the melting of [BMIM]BF_4 suggests the confinement of the ionic liquid in the pores. (b) Representative QENS spectra (collected for 3 h) of [BMIM]BF_4 in the bulk and confined within the porous carbon fibers at Q = 0.7 $Å^{-1}$ with normalized maximum intensity (n = 1). (c) Extraction of HWHM at each Q allows for the determination of the Q-dependence of HWHM. The Q-dependence of HWHM allows for the calculation of the diffusion coefficient of the [BMIM] cation. Error bars in (a) represent one standard deviation. When not visible (in (b) and (c)), the error bars are within the symbols. The total number of neutrons detected per sample (n) varies between 3.5×10^6 and 5.2×10^6.

with the unchanged pore size, suggest that the ionic liquid blocked some sorption sites. The ionic liquid likely formed plugs in the pore rather than coatings on the wall (Figure 2d), which would lead to a reduction in the pore sizes. If the adsorbate (i.e., N_2 and CO_2) is soluble in the ionic liquid, the physisorption will give a falsely large surface area because the adsorbate is dissolved in the liquid rather than adsorbed on the pore surfaces. Considering the low solubility of N_2 in [BMIM]BF_4, similar to that in [BMIM]PF_6,[25] the gas dissolution effect is unlikely to affect the N_2 results. Physisorption of CO_2 showed the same trend, and thus the effect of CO_2 solubility was also negligible. Regardless, the physisorption serves as a qualitative means for confirming the presence of the ionic liquid in the fibers.

Relying on the high incoherent scattering cross section of hydrogen atoms,[26] quasi-elastic neutron scattering (QENS) is the technique of choice to explore the dynamics in systems that contain hydrogen atoms.[27,28] Since the cation of

https://doi.org/10.1021/acsami.2c12755
ACS Appl. Mater. Interfaces 2022, 14, 36980−36986

[BMIM]BF_4 is rich in hydrogen atoms, the dynamics of the bulk and PCF-confined BMIM ions could be measured using QENS. First, temperature-dependent energy-resolved elastic scans were conducted using high-flux backscattering spectrometer[29] on the confined [BMIM]BF_4 (Figure 3a). The elastic intensity of the confined ionic liquid was significantly higher at 10 K compared to the bare PCF matrix, suggesting the presence of the ionic liquid in the pores (in agreement with the physisorption data). [BMIM]BF_4 melts at 198 K, and at this temperature, the elastic intensity would show a step corresponding to a thermal phase transition.[30,31] The absence of a step in all elastic scattering spectra collected for [BMIM]BF_4 in the fibers, however, confirmed the confinement of [BMIM]BF_4 within the pores and the disruption of the ionic liquid's lattice structure.[32] Additionally, the absence of water and acetonitrile in [BMIM]BF_4 inside the pores was confirmed by the lack of any significant step at 273 K (water's freezing point) or 228 K (acetonitrile's freezing point). Figure 3 (main panel) shows the representative quasi-elastic spectra measured using backscattering silicon spectrometer[33] and the corresponding model fits (See the SI for details) of the bulk and confined [BMIM]BF_4, together with the instrument resolution. Even though the spectrum collected from the bulk [BMIM]-BF_4 appeared to exhibit more pronounced QENS broadening than that for the confined [BMIM]BF_4, the data analysis (using eq S1, SI) demonstrates that the mobile ions in the confined ionic liquid (those that contributed to the QENS signal rather than the elastic line) gave rise to a relatively broader signal. In other words, while the overall QENS intensity for the PCFs with [BMIM]BF_4 was lower due to immobilized ions that contributed only to the elastic scattering, those that remained mobile exhibited higher diffusivity than the ions in the bulk [BMIM]BF_4 despite its overall higher QENS intensity. The half-width at half-maximum (HWHM) of the slow components of the bulk and confined [BMIM]BF_4 (Figure 3b) showed a nonlinear dependence on Q,[2] which corresponded to a long-range translational mobility of the ions.[34,35] Therefore, the translational diffusion coefficient (D) of the cation in the bulk liquid was determined using a jump diffusion model (diffusion with a relaxation time), giving a value of $(0.73 \pm 0.06) \times 10^{-10}$ m^2 s^{-1}, in agreement with similar systems in a previous report.[34] The diffusion dynamics of the confined cation were found to be nonhomogeneous, i.e., non-exponential, requiring the introduction of an exponent $\alpha(Q) = 0.5$ (a typical value used for other small molecule glass formers)[36,37] to fit the data using a Cole−Cole distribution function (see the SI for details). This functional form has been employed successfully in many confined systems.[38,39] For the confined [BMIM] cation, the diffusion coefficient value was determined to be $(5.1 \pm 1.1) \times 10^{-10}$ m^2 s^{-1}, about ∼7 times greater than that of the unconfined bulk ionic liquid.

Although this enhanced diffusion behavior of the confined fluid has been witnessed in other materials,[14] the amount of enhancement is unprecedented. Compared to all available materials to date, the porous carbon fibers show the largest increase in diffusion coefficient for the [BMIM] cation (Table 1), likely owing to a few features of PCFs.[40] Our porous carbon fibers are hydrophilic due to the high content of surface N and O heteroatoms, similar to our previous reports.[20,41] The heteroatom content of the PCFs contrasts with the rest of the works cited in Table 1. Due to the hydrophilic PCFs, ions stabilize along the surface of the pores. The stabilized surface-layer ions decouple from the ions in the diffuse layer and prevent effective long-range ion packing. Owing to reduced IL packing, the diffusion layers within the mesopores exhibit lower viscosity and friction. The balance of the pore volume and the packed layers becomes imperative for enhanced diffusion within the carbon matrix.[42] The mesopore size allowed a significant amount of confined ionic liquid to exist in the diffuse layer rather than the adsorbed layer. The lack of a transition in the elastic scan across the examined temperature range (Figure 3a) indicated that the disrupted lattice structure extends across the whole pore, frustrating the ion packing. Thus, ions in the diffuse layer do not freeze between 10 and 300 K despite the typical freezing point of [BMIM]BF_4 being 198 K. The disruption of the lattice, in combination with the reduced friction between the adsorbed ions and the confined diffuse-layer ions, leads to the exceptionally high diffusion coefficient. Our results match the observations of Dyatkin et al.,[23] where the ions inside the 0.8 nm micropores were immobile and the high diffusion coefficient was attributed to the inner ion layers inside mesopores. Ghoufi et al. also found a large increase in diffusion of the [BMIM] cation in 1.3 nm diameter pores of (20,20) carbon nanotubes (CNTs), owing to a small friction.[19] Additionally, Ohba et al. found a reduction in ionic liquid viscosity within CNTs, and the ions revealed ordered coordination with CNT walls when the micropore diameters were 0.63, 0.86, 1.28, and 1.73 nm.[43] Similarly, the ion diffusion in PCFs also showed a positive correlation with micropore sizes of 0.55, 0.86, and 1.23 nm (Figure 2c). Ionic liquid diffusion in mesoporous carbon for supercapacitors was also studied by Liu et al. who found a juxtaposition between pore size and electrochemical performance limited by ion diffusion.[44] The fastest ion diffusion in mesoporous carbon was found when the mesopore sizes were 13.9 nm for cations with a size of 7.6 Å, in agreement with the favorable mesopore size of 13.6 nm in PCFs herein.[44] In addition, the surface interactions resulting from heteroatoms further improved the ion diffusion characteristics, in consistency with the previous finding that the heteroatomic species of N-X and O/O-H provide a layered surface for aligned cations to facilitate rapid ionic diffusion.[45,46]

Table 1. Diffusion Coefficient of [BMIM] Cations in Porous Carbon Fibers in Comparison with those in Other Materials[a]

systems	D_{BMIM} (10^{-10} m^2s^{-1})	pore diameter(nm)	method
carbon-derived carbon[32]	0.52	0.8/3.1	QENS
mesoporous carbon[34]	2.55	8.8	QENS
vertically aligned CNT[40]	0.31	4	PFG-NMR
silicon carbide−carbon-derived carbon[23]	2.32	0.8	QENS
CNT (20,20)[19]	2.86	1.3	MD
CNT (40,40)[19]	0.43	2.7	MD
CNT (34,0)[19]	0.41	1.3	MD
graphene sheets[19]	0.01	2.7	MD
porous carbon fibers	5.1	13.6	QENS

[a]All diffusion coefficients are based on long-range diffusion at 298/300 K. CNT, carbon nanotubes; PFG-NMR, pulse field gradient nuclear magnetic resonance; MD, molecular dynamics modeling.

3. CONCLUSIONS

In summary, advanced QENS measurements show that the block copolymer-based porous carbon fibers have exceptional

https://doi.org/10.1021/acsami.2c12755
ACS Appl. Mater. Interfaces 2022, 14, 36980−36986

ion diffusion properties. The confined ions exhibit a 7-fold increase in the diffusion coefficient. Attachment of the cations to the pore wall (which are not mobile within the sensitivity of the instrument) contributes to the elastic incoherent scattering fraction, which, in turn, can be related to the electrochemical capacitance of porous materials. The fast diffusivity of the cations away from the wall could contribute to the high-rate capability of the porous carbon fibers for use in supercapacitors as well as fast charging/discharging in batteries. The exceptional ion diffusion also holds great promise for fast mass transport in electrochemical catalysis. Last, tunability in PCF properties based on the initial block copolymer offers opportunities to control hydrophilicity, pore size, and other characteristics to further adjust the confinement effect. Therefore, the block copolymer-based porous carbon fibers represent an outstanding platform material for electrochemical applications.

4. EXPERIMENTAL SECTION

4.1. Fiber Characterization. A Micromeritics-3Flex pore analyzer was used to determine the surface areas and porosities of the porous carbon fibers. A sample of ∼50 mg fibers was placed into a physisorption tube and degassed at 300 °C for 10 h to remove oxygen and any adsorbed volatile species. The mass of the fibers was recorded by subtracting post-degas mass from the mass of the empty tube. CO_2-sorption tests were carried out using CO_2 and dipping the physisorption tube into a Dewar containing ice water (273 K). N_2 sorption tests were carried out using N_2 and dipping the physisorption tube into a Dewar containing liquid nitrogen (77 K). One sample (n = 1) of PCF with and without ionic liquid was used for both N_2 and CO_2 physisorption tests.

Fiber morphology was characterized using electron microscopy imaging. Scanning electron microscopy (SEM, LEO Zeiss 1550) images were taken using an accelerating voltage of 3 kV and a working distance of 2.9 mm (Figure 1b,c). To prepare for transmission electron microscopy (TEM), PCFs were dispersed in deionized water by ultrasonication. A drop of the suspension was then spread on a carbon-coated copper TEM grid, followed by drying on a hot plate at 60 °C for 30 min. TEM images were then collected on a probe-corrected transmission electron microscope (FEI ChemiSTEM 80-200) operating at 200 kV (Figure 1d).

4.2. Vacuum Infiltration of [BMIM]BF_4 into Pores. Porous carbon fibers were suspended in a solution of [BMIM]BF_4 in acetonitrile (0.015 mg/mL). The suspension was stirred for 3 h in a glovebox with an argon atmosphere. Afterward, the suspension was transferred to a vacuum oven to remove acetonitrile at 80 °C, leaving behind the [BMIM]BF_4 inside the pores of porous carbon fibers.

4.3. Neutron Scattering Experiments. Neutron scattering experiments were performed using two neutron backscattering spectrometers, with the sample temperature controlled using closed-cycle refrigerators. Fixed window scans of the elastic scattering intensity were performed using the High-Flux Backscattering Spectrometer (HFBS)[29] at the NIST Center for Neutron Research in Gaithersburg, MD. HFBS has an energy resolution of 0.8 μeV (full width at half maximum, FWHM). The instrument covers a momentum transfer vector (Q) range of 0.25 to 1.74 Å^{-1} and an energy transfer range of ±16 μeV. Elastic intensity spectra from the 0.25 mm thick samples, which were loaded in flat plate aluminum sample holders, were collected with a heating rate of 1 K/min. The data were reduced using DAVE software[47] available at NIST-NCNR.

Quasielastic neutron scattering (QENS) measurements of both the bulk and confined ionic liquid were carried out using the Backscattering Silicon Spectrometer (BASIS)[33] at the Spallation Neutron Source in the Oak Ridge National Laboratory, Oak Ridge, TN. The instrument was operated at its standard configuration, which provides an energy resolution of 3.7 μeV (FWHM), using a bandwidth of incoming neutrons centered at 6.4 Å and covering an energy range of ±100 μeV. This setup of the instrument spans a Q range of 0.2 to 2.0 Å^{-1}. QENS spectra were collected at 300 K along with the sample-specific instrument resolution at 20 K. Mantid software[48] was used for the data reduction. The analysis of the data was performed using the DAVE package. The errors on the parameters after QENS peak fitting are obtained from the chi-squared minimization and represent one standard deviation. The number of samples was n = 1 for all compositions (one PCF sample with ionic liquid, one PCF sample without ionic liquid, and one sample of pure ionic liquid. The total number of neutrons detected per sample varies between 3.5×10^6 and 5.2×10^6.

ASSOCIATED CONTENT

Supporting Information

The Supporting Information is available free of charge at https://pubs.acs.org/doi/10.1021/acsami.2c12755.

SEC and TGA traces; ^{1}H NMR and XPS spectra (PDF)

AUTHOR INFORMATION

Corresponding Authors

Naresh C. Osti − *Neutron Scattering Division, Oak Ridge National Laboratory, Oak Ridge, Tennessee 37831, United States;* orcid.org/0000-0002-0213-2299; Email: ostinc@ornl.gov

Guoliang Liu − *Department of Chemistry and Macromolecules Innovation Institute, Virginia Tech, Blacksburg, Virginia 24061, United States;* orcid.org/0000-0002-6778-0625; Email: gliu1@vt.edu

Authors

John P. Elliott − *Department of Chemistry, Virginia Tech, Blacksburg, Virginia 24061, United States;* orcid.org/0000-0003-4560-8493

Madhusudan Tyagi − *NIST Center for Neutron Research, National Institute of Standards and Technology, Gaithersburg, Maryland 20899, United States; Department of Materials Science, University of Maryland, Maryland 20742, United States*

Eugene Mamontov − *Neutron Scattering Division, Oak Ridge National Laboratory, Oak Ridge, Tennessee 37831, United States;* orcid.org/0000-0002-5684-2675

Lifeng Liu − *International Iberian Nanotechnology Laboratory (INL), 4715-330 Braga, Portugal;* orcid.org/0000-0003-2732-7399

Joel M. Serrano − *Department of Chemistry, Virginia Tech, Blacksburg, Virginia 24061, United States;* orcid.org/0000-0002-1508-5508

Ke Cao − *Macromolecules Innovation Institute, Virginia Tech, Blacksburg, Virginia 24061, United States;* orcid.org/0000-0001-7204-7455

Complete contact information is available at: https://pubs.acs.org/10.1021/acsami.2c12755

Notes

The authors declare no competing financial interest.

ACKNOWLEDGMENTS

This article contains studies supported by the National Science Foundation under grant no. DMR-1752611 through the CAREER award and the American Chemical Society Petroleum Research Foundation Doctoral New Investigator Award. Work at ORNL's Spallation Neutron Source was sponsored by the Scientific User Facilities Division, Office of Basic Energy Sciences, US Department of Energy. The Oak

Ridge National Laboratory is managed by UT-Battelle, LLC, for US DOE under contract no. DEAC05-00OR22725. Experiments on HFBS at NIST Center for Neutron Research (NCNR) were supported in part by the National Science Foundation under agreement no. DMR-2010792. Certain commercial material suppliers are identified in this paper to foster understanding. Such identification does not imply recommendation or endorsement by the National Institute of Standards and Technology, nor does it imply that the materials or equipment identified are necessarily the best available for the purpose.

REFERENCES

(1) Kim, S.; Ju, M.; Lee, J.; Hwang, J.; Lee, J. Polymer Interfacial Self-Assembly Guided Two-Dimensional Engineering of Hierarchically Porous Carbon Nanosheets. *J. Am. Chem. Soc.* **2020**, *142*, 9250−9257.

(2) Rouhani, F.; Rafizadeh-Masuleh, F.; Morsali, A. Highly Electroconductive Metal-Organic Framework: Tunable by Metal Ion Sorption Quantity. *J. Am. Chem. Soc.* **2019**, *141*, 11173−11182.

(3) Yu, M.; Chandrasekhar, N.; Raghupathy, R. K. M.; Ly, K. H.; Zhang, H.; Dmitrieva, E.; Liang, C.; Lu, X.; Kuhne, T. D.; Mirhosseini, H.; Weidinger, I. M.; Feng, X. A High-Rate Two-Dimensional Polyarylimide Covalent Organic Framework Anode for Aqueous Zn-Ion Energy Storage Devices. *J. Am. Chem. Soc.* **2020**, *142*, 19570−19578.

(4) Salim, N. V.; Mateti, S.; Cizek, P.; Hameed, N.; Parameswaranpillai, J.; Fox, B. Large, Mesoporous Carbon Nanoparticles with Tunable Architectures for Energy Storage. *ACS Appl. Nano Mater.* **2019**, *2*, 1727−1736.

(5) Zhong, M.; Kim, E. K.; McGann, J. P.; Chun, S. E.; Whitacre, J. F.; Jaroniec, M.; Matyjaszewski, K.; Kowalewski, T. Electrochemically Active Nitrogen-Enriched Nanocarbons with Well-Defined Morphology Synthesized by Pyrolysis of Self-Assembled Block Copolymer. *J. Am. Chem. Soc.* **2012**, *134*, 14846−14857.

(6) Rogers, R. D.; Seddon, K. R. Ionic Liquids–Solvents of the Future? *Science* **2003**, *302*, 792−793.

(7) Wasserscheid, P. Chemistry: Volatile Times for Ionic Liquids. *Nature* **2006**, *439*, 797.

(8) Liang, Y.; Liu, H.; Li, Z.; Fu, R.; Wu, D. In Situ Polydopamine Coating-Directed Synthesis of Nitrogen-Doped Ordered Nanoporous Carbons with Superior Performance in Supercapacitors. *J. Mater. Chem. A* **2013**, *1*, 15207.

(9) Lin, R.; Huang, P.; Ségalini, J.; Largeot, C.; Taberna, P. L.; Chmiola, J.; Gogotsi, Y.; Simon, P. Solvent Effect on the Ion Adsorption from Ionic Liquid Electrolyte into Sub-Nanometer Carbon Pores. *Electrochim. Acta* **2009**, *54*, 7025−7032.

(10) Hayes, R.; Warr, G. G.; Atkin, R. Structure and Nanostructure in Ionic Liquids. *Chem. Rev.* **2015**, *115*, 6357−6426.

(11) Rajput, N. N.; Monk, J.; Singh, R.; Hung, F. R. On the Influence of Pore Size and Pore Loading on Structural and Dynamical Heterogeneities of an Ionic Liquid Confined in a Slit Nanopore. *J. Phys. Chem. C* **2012**, *116*, 5169−5181.

(12) Singh, M. P.; Singh, R. K.; Chandra, S. Ionic Liquids Confined in Porous Matrices: Physicochemical Properties and Applications. *Prog. Mater. Sci.* **2014**, *64*, 73−120.

(13) Zhou, Z.; Liu, T.; Khan, A.; Liu, G. Block Copolymer−Based Porous Carbon Fibers. *Sci. Adv.* **2019**, *5*, No. eaau6852.

(14) Liu, T.; Serrano, J.; Elliott, J.; Yang, X.; Cathcart, W.; Wang, Z.; He, Z.; Liu, G. Exceptional Capacitive Deionization Rate and Capacity by Block Copolymer-Based Porous Carbon Fibers. *Sci. Adv.* **2020**, *6*, No. eaaz0906.

(15) Liu, T.; Liu, G. Block Copolymer-Based Porous Carbons for Supercapacitors. *J. Mater. Chem. A* **2019**, *7*, 23476−23488.

(16) Futamura, R.; Iiyama, T.; Takasaki, Y.; Gogotsi, Y.; Biggs, M. J.; Salanne, M.; Segalini, J.; Simon, P.; Kaneko, K. Partial Breaking of the Coulombic Ordering of Ionic Liquids Confined in Carbon Nanopores. *Nat. Mater.* **2017**, *16*, 1225−1232.

(17) Gutiérrez, A.; Atilhan, M.; Alcalde, R.; Trenzado, J. L.; Aparicio, S. Insights on the Mixtures of Imidazolium Based Ionic Liquids with Molecular Solvents. *J. Mol. Liq.* **2018**, *255*, 199−207.

(18) Peng, J.; Zhang, W.; Yu, P.; Pang, H.; Zheng, M.; Dong, H.; Hu, H.; Xiao, Y.; Liu, Y.; Liang, Y. Improved Ion-Diffusion Performance by Engineering an Ordered Mesoporous Shell in Hollow Carbon Nanospheres. *Chem. Commun.* **2020**, *56*, 2467−2470.

(19) Ghoufi, A.; Szymczyk, A.; Malfreyt, P. Ultrafast Diffusion of Ionic Liquids Confined in Carbon Nanotubes. *Sci. Rep.* **2016**, *6*, 28518.

(20) Serrano, J. M.; Liu, T.; Khan, A. U.; Botset, B.; Stovall, B. J.; Xu, Z.; Guo, D.; Cao, K.; Hao, X.; Cheng, S.; Liu, G. Composition Design of Block Copolymers for Porous Carbon Fibers. *Chem. Mater.* **2019**, *31*, 8898−8907.

(21) Miao, L.; Duan, H.; Liu, M.; Lu, W.; Zhu, D.; Chen, T.; Li, L.; Gan, L. Poly(Ionic Liquid)-Derived, N, S-Codoped Ultramicroporous Carbon Nanoparticles for Supercapacitors. *Chem. Eng. J.* **2017**, *317*, 651−659.

(22) Kondrat, S.; Wu, P.; Qiao, R.; Kornyshev, A. A. Accelerating Charging Dynamics in Subnanometre Pores. *Nat. Mater.* **2014**, *13*, 387−393.

(23) Dyatkin, B.; Osti, N. C.; Gallegos, A.; Zhang, Y.; Mamontov, E.; Cummings, P. T.; Wu, J.; Gogotsi, Y. Electrolyte Cation Length Influences Electrosorption and Dynamics in Porous Carbon Supercapacitors. *Electrochim. Acta* **2018**, *283*, 882−893.

(24) Dyatkin, B.; Mamontov, E.; Cook, K. M.; Gogotsi, Y. Capacitance, Charge Dynamics, and Electrolyte Surface Interactions in Functionalized Carbide Derived Carbon Electrodes. *Prog. Nat. Sci.* **2015**, *25*, 631−641.

(25) Anthony, J. L.; Maginn, E. J.; Brennecke, J. F. Solubilities and Thermodynamic Properties of Gases in the Ionic Liquid 1-N-Butyl-3-Methylimidazolium Hexafluorophosphate. *J. Phys. Chem. B* **2002**, *106*, 7315−7320.

(26) Bee, M., *Quasielastic Neutron Scattering: Principles and Applications in Solid State Chemistry, Biology, and Materials Science*. Adam Hilger, Bristol: 1998; p 28.

(27) Osti, N. C.; Mamontov, E. Microscopic Dynamics in Room-Temperature Ionic Liquids Confined in Materials for Supercapacitor Applications. *Sustainable Energy Fuels* **2020**, *4*, 1554−1576.

(28) Osti, N. C.; Cote, A.; Mamontov, E.; Ramirez-Cuesta, A.; Wesolowski, D. J.; Diallo, S. O. Characteristic Features of Water Dynamics in Restricted Geometries Investigated with Quasi-Elastic Neutron Scattering. *Chem. Phys.* **2016**, *465*, 1−8.

(29) Meyer, A.; Dimeo, R.; Gehring, P.; Neumann, D. The High-Flux Backscattering Spectrometer at the Nist Center for Neutron Research. *Rev. Sci. Instrum.* **2003**, *74*, 2759−2777.

(30) Mamontov, E.; Luo, H. M.; Dai, S. Proton Dynamics in N,N,N',N'-Tetramethylguanidinium Bis(Perfluoroethylsulfonyl)Imide Protic Ionic Liquid Probed by Quasielastic Neutron Scattering. *J. Phys. Chem. B* **2009**, *113*, 159−169.

(31) Prisk, T. R.; Tyagi, M.; Sokol, P. E. Dynamics of Small-Molecule Glass Formers Confined in Nanopores. *J. Chem. Phys.* **2011**, *134*, 114506.

(32) Osti, N. C.; Dyatkin, B.; Thompson, M. W.; Tiet, F.; Zhang, P. F.; Dai, S.; Tyagi, M.; Cummings, P. T.; Gogotsi, Y.; Wesolowski, D. J.; Mamontov, E. Influence of Humidity on Performance and Microscopic Dynamics of an Ionic Liquid in Supercapacitor. *Phys. Rev. Mater.* **2017**, *1*, No. 035402.

(33) Mamontov, E.; Herwig, K. W. A Time-of-Flight Backscattering Spectrometer at the Spallation Neutron Source, Basis. *Rev. Sci. Instrum.* **2011**, *82*, No. 085109.

(34) Chathoth, S. M.; Mamontov, E.; Dai, S.; Wang, X.; Fulvio, P. F.; Wesolowski, D. J. Fast Diffusion in a Room Temperature Ionic Liquid Confined in Mesoporous Carbon. *Europhys. Lett.* **2012**, *97*, 66004.

(35) Chathoth, S. M.; Mamontov, E.; Fulvio, P. F.; Wang, X.; Baker, G. A.; Dai, S.; Wesolowski, D. J. An Unusual Slowdown of Fast Diffusion in a Room Temperature Ionic Liquid Confined in Mesoporous Carbon. *Europhys. Lett.* **2013**, *102*, 16004.

https://doi.org/10.1021/acsami.2c12755
ACS Appl. Mater. Interfaces 2022, 14, 36980−36986

(36) Borjesson, L.; Elmroth, M.; Torell, L. M. Neutron and Light-Scattering Study of Relaxation Dynamics in a Glass-Forming Fragile Molecular Liquid. *Chem. Phys.* **1990**, *149*, 209−220.
(37) Tyagi, M.; Arbe, A.; Alvarez, F.; Colmenero, J.; Gonzalez, M. Short-Range Order and Collective Dynamics of Poly(Vinyl Acetate): A Combined Study by Neutron Scattering and Molecular Dynamics Simulations. *J. Chem. Phys.* **2008**, *129*, 224903−224914.
(38) Dyatkin, B.; Osti, N. C.; Zhang, Y.; Wang, H.-W.; Mamontov, E.; Heller, W. T.; Zhang, P.; Rother, G.; Cummings, P. T.; Wesolowski, D. J.; Gogotsi, Y. Ionic Liquid Structure, Dynamics, and Electrosorption in Carbon Electrodes with Bimodal Pores and Heterogeneous Surfaces. *Carbon* **2018**, *129*, 104−118.
(39) Osti, N. C.; Dyatkin, B.; Gallegos, A.; Voneshen, D.; Keum, J. K.; Littrell, K.; Zhang, P. F.; Dai, S.; Wu, J. Z.; Gogotsi, Y.; Mamontov, E. Cation Molecular Structure Affects Mobility and Transport of Electrolytes in Porous Carbons. *J. Electrochem. Soc.* **2019**, *166*, A507−A514.
(40) Berrod, Q.; Ferdeghini, F.; Judeinstein, P.; Genevaz, N.; Ramos, R.; Fournier, A.; Dijon, J.; Ollivier, J.; Rols, S.; Yu, D.; Mole, R. A.; Zanotti, J. M. Enhanced Ionic Liquid Mobility Induced by Confinement in 1d Cnt Membranes. *Nanoscale* **2016**, *8*, 7845−7848.
(41) Zhou, Z.; Liu, T.; Khan, A. U.; Liu, G. Controlling the Physical and Electrochemical Properties of Block Copolymer-Based Porous Carbon Fibers by Pyrolysis Temperature. *Mol. Syst.* **2020**, *5*, 153−165.
(42) Liu, T.; Zhang, F.; Song, Y.; Li, Y. Revitalizing Carbon Supercapacitor Electrodes with Hierarchical Porous Structures. *J. Mater. Chem. A* **2017**, *5*, 17705−17733.
(43) Ohba, T.; Chaban, V. V. A Highly Viscous Imidazolium Ionic Liquid inside Carbon Nanotubes. *J. Phys. Chem. B* **2014**, *118*, 6234−6240.
(44) Liu, Y.; Zhang, H.; Song, H.; Noonan, O.; Liang, C.; Huang, X.; Yu, C. Single-Layered Mesoporous Carbon Sandwiched Graphene Nanosheets for High Performance Ionic Liquid Supercapacitors. *J. Phys. Chem. C* **2017**, *121*, 23947−23954.
(45) Choi, W.; Ulissi, Z. W.; Shimizu, S. F.; Bellisario, D. O.; Ellison, M. D.; Strano, M. S. Diameter-Dependent Ion Transport through the Interior of Isolated Single-Walled Carbon Nanotubes. *Nat. Commun.* **2013**, *4*, 2397.
(46) Elverfeldt, C. P.; Lee, Y. J.; Froba, M. Selective Control of Ion Transport by Nanoconfinement: Ionic Liquid in Mesoporous Resorcinol-Formaldehyde Monolith. *ACS Appl. Mater. Interfaces* **2019**, *11*, 24423−24434.
(47) Azuah, R. T.; Kneller, L. R.; Qiu, Y. M.; Tregenna-Piggott, P. L. W.; Brown, C. M.; Copley, J. R. D.; Dimeo, R. M. Dave: A Comprehensive Software Suite for the Reduction, Visualization, and Analysis of Low Energy Neutron Spectroscopic Data. *J. Res. Natl. Inst.. Stand. Technol.* **2009**, *114*, 341−358.
(48) Arnold, O.; Bilheux, J. C.; Borreguero, J. M.; Buts, A.; Campbell, S. I.; Chapon, L.; Doucet, M.; Draper, N.; Leal, R. F.; Gigg, M. A.; Lynch, V. E.; Markvardsen, A.; Mikkelson, D. J.; Mikkelson, R. L.; Miller, R.; Palmen, K.; Parker, P.; Passos, G.; Perring, T. G.; Peterson, P. F.; Ren, S.; Reuter, M. A.; Sayici, A. T.; Taylor, J. W.; Taylor, R. J.; Tolchenoy, R.; Zhou, W.; Zikoysky, J. Mantid-Data Analysis and Visualization Package for Neutron Scattering and Mu Sr Experiments. *Nuclear Instruments & Methods in Physics Research Section a-Accelerators Spectrometers Detectors and Associated Equipment* **2014**, *764*, 156−166.

https://doi.org/10.1021/acsami.2c12755
ACS Appl. Mater. Interfaces 2022, 14, 36980−36986